Hindawi
Mathematical Problems in Engineering
Volume 2021, Article ID 6682659, 11 pages
https://doi.org/10.1155/2021/6682659

Research Article

Particle Swarm Optimization Algorithm in Numerical Simulation of Saturated Rock Slope Slip

Bowen Liu,[1] **Zhenwei Wang**,[2] **and Xiaoyong Zhong**[3]

[1]*School of Energy and Mining Engineering, China University of Mining and Technology, Beijing 100083, China*
[2]*School of Civil Engineering, North China University of Technology, Beijing 100144, China*
[3]*Hulunbuir Dongming Mining Co., Ltd., Hulunbuir 021500, Inner Mongolia, China*

Correspondence should be addressed to Bowen Liu; bqt1800101016@student.cumtb.edu.cn and Zhenwei Wang; kingzw627@163.com

Received 17 December 2020; Revised 13 January 2021; Accepted 22 February 2021; Published 17 March 2021

Academic Editor: Sang-Bing Tsai

With the continuous popularization and development of highway traffic in mountainous areas, the number of rock slopes is also increasing. In order to improve the stability of rock slope and reduce the harm caused by slope slip, this paper carries out numerical simulation of rock slope sliding based on particle swarm optimization algorithm. Firstly, this paper combines the differential evolution algorithm and simplex method to improve the global and local search ability of particle swarm optimization (PSO) algorithm and analyzes the performance of the algorithm. ABAQUS software is used to simulate rock slope sliding, the finite element method is used to analyze the stability of rock slope, and LS-DYNA program is used to simulate rockfall impact rock slope. During the numerical simulation, the improved algorithm is used to analyze all the data. Experimental data show that the improved PSO algorithm converges after nearly 100 iterations and the convergence speed and optimization accuracy are high. In the numerical simulation, the average failure probability of the left and right sides of the main section at the top, middle, and foot of the slope is 0.0820 and 0.0723, 0.0772 and 0.0492, and 0.0837 and 0.0677, respectively, indicating that the overall instability probability of the left side of the rock slope is higher than that of the right side. The rock slope with the same direction through joint is mainly affected by the joint at the toe of the slope, the rock slope with reverse through joint is mainly affected by the joint in the slope, and the sliding occurs from the middle to both ends. In addition, with the increase of the size and height of rockfall, the total energy of rock slope is also increasing, and the possibility and degree of rock slope sliding are higher. This shows that the improved particle swarm optimization algorithm can effectively analyze some factors affecting slope slip in numerical simulation of saturated rock slope slip.

1. Introduction

1.1. Background Significance. In mountainous areas, because of the development of traffic and economy, the construction of roads and buildings, there are a large number of rock slopes with potential safety hazards. The stability of rock slope has a direct impact on the safety of traffic and residents in nearby areas. Once landslide disaster occurs, it will bring huge economic losses and security threats [1, 2]. Therefore, it is necessary to detect and predict the slip of rock slope in real time. Numerical simulation of slip of rock slope can effectively analyze the stability of rock slope, but it requires a large amount of calculation in data analysis. Particle swarm optimization algorithm has the advantages of simple operation and fast convergence speed, which can improve the efficiency of analysis [3, 4]. Therefore, this paper proposes an improved algorithm based on particle swarm optimization algorithm and applies it to the numerical simulation of slope sliding, which provides a new idea for solving the engineering problem of rock slope stability.

1.2. Related Work. Particle swarm optimization (PSO) is widely used in many fields because of its advantages of simple operation and fast convergence speed. Mohamadi proposed a multiobjective stochastic programming model to

establish an earthquake response plan integrating predisaster and postdisaster decision-making. Aiming at this model, he proposed a new multiobjective particle swarm optimization algorithm and designed binary particle swarm optimization algorithm and continuous particle swarm optimization algorithm based on genotype sound pattern to deal with binary position and other continuous decision variables. Zhang et al. proposed a chaos multiobjective particle swarm optimization algorithm based on particle swarm optimization algorithm and invasive weed algorithm and evaluated the performance of the method through four common two-objective problems [5]. Their improvement of particle swarm optimization algorithm provides a reference for this study, but, after the improvement of the algorithm, they did not carry out more comparative analysis to prove the effectiveness of the improvement.

The problem of rock slope sliding has always been the focus of engineering. Wang et al. studied the sliding failure of jointed rock slope caused by mechanical degradation of rock mass under dry wet cycle [6]. According to the mechanical parameters of reservoir limestone under different drying and wetting cycles, he used the discrete element method to analyze the slippage failure mode of the North-South slope of the Yellow River in the Three Gorges Reservoir area. Zhuang et al. studied the sliding mechanism of Earth rock slope by using transparent soil technology and considered the influence of rock joint roughness coefficient, soil angle, rock angle, and soil layer thickness on slope stability [7]. He also used particle image velocimetry and laser speckle technology to obtain the deformation characteristics of rock and soil slope. Although their research on rock slope slip is effective, there are still some deficiencies in the technology of predicting the occurrence time of rock slope slip.

1.3. Innovative Points in This Paper. In order to conduct more accurate numerical simulation of rock slope slip, improve the stability of rock slope, and reduce the economic and life hazards brought by rock slope sliding, this paper analyzes the rock slope sliding based on particle swarm optimization algorithm. The innovation points of this study are as follows: (1) based on the differential evolution algorithm and simplex method, the standard particle swarm optimization algorithm is improved, which improves the global and local search ability of the particle swarm optimization algorithm in the early and late iterations [8]. It is found that the proposed algorithm has faster convergence speed and higher optimization accuracy. (2) ABAQUS software is used for numerical simulation of rock slope sliding, and finite element method is used for analysis. The top, middle, and foot of slope are selected as feature points. It is found that the failure probability of the left side of the rock slope model is higher than that of the right side. (3) LS-DYNA program was used to construct the slope model of rockfall impact rock, and numerical simulation was carried out. It was found that the size and height of rockfall were proportional to the possibility of slope slip.

2. Particle Swarm Optimization Algorithm and Sliding Analysis of Saturated Rock Slope

2.1. Particle Swarm Optimization Algorithm

2.1.1. Mathematical Model and Process. The particle swarm optimization (PSO) algorithm simulates the foraging behavior of birds, taking birds as potential optimal solutions, that is, particles [9]. Because the mass and volume of the birds are ignored, the number of parameters is small and easy to operate. Local and global optimal values are found through population iterative optimization [10]. Assuming that there are m particles in the solution space, the expressions of the position and velocity of the I-th particle in the n-dimensional space are shown in the following formulae:

$$P_i = (p_{i1}, p_{i2}, \ldots, p_{iN}), \tag{1}$$

$$V_i = (v_{i1}, v_{i2}, \ldots, v_{iN}), \tag{2}$$

where $i = 1, 2, \ldots, M$. The historical optimal position of the particle is H_{best} and the global optimal position is G_{best}. Formulae (1) and (2) are improved by introducing inertia weight and learning factor. The position and speed of particles are updated as shown in the following formulae:

$$P_i^{e+1} = P_i^e + V_i^{e+1}, \tag{3}$$

$$V_i^{e+1} = \varpi V_i^e + s_1 r_1 (H_{\text{best}} - P_i^e) + s_2 r_2 (G_{\text{best}} - P_i^e), \tag{4}$$

where ϖ is the inertia weight, e is the current iteration number, s_1, s_2 are the learning factor, and r_1, r_2 are the random number between [0, 1]. ϖV_i^e is the inertial motion of the previous generation of particles, $s_1 r_1 (H_{\text{best}} - P_i^e)$ is the particle's own position, $s_2 r_2 (G_{\text{best}} - P_i^e)$ represents the group information sharing, and the three parts restrain each other to achieve balance. The dynamic value of inertia weight ϖ is shown in the following formula:

$$\varpi(e) = \varpi_{\max} - \frac{e}{\max ie} (\varpi_{\max} - \varpi_{\min}). \tag{5}$$

The running process of particle swarm optimization algorithm is as follows:

As shown in Figure 1, the parameters of the particle swarm are initialized first, and then the fitness value of each particle is calculated. The third step is to calculate the historical optimal value and the global optimal value of the particle to determine whether the particle speed is less than or beyond the speed constraint, and, if so, set it to the maximum or minimum speed. The fourth step is to determine whether the termination conditions are met. If not, the fitness value of particles is recalculated, the position and velocity of particles are updated, and the following steps are repeated.

2.1.2. Influence of Algorithm Parameter Setting. The parameters of PSO algorithm directly affect the performance of PSO algorithm, so we must consider it again when choosing

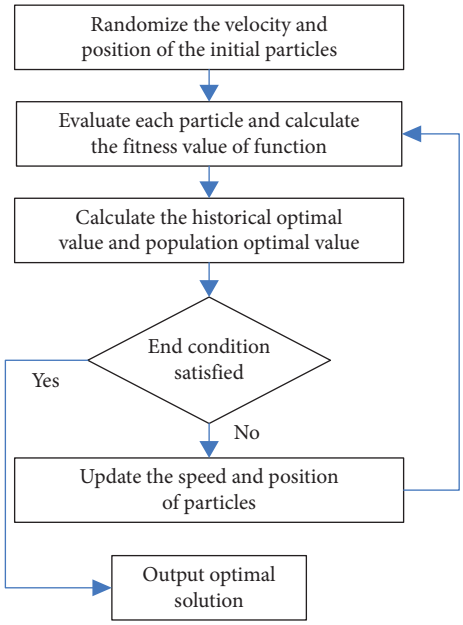

Figure 1: Flow chart of particle swarm optimization algorithm.

parameters, in order to improve the convergence speed of the algorithm and find the global optimal solution. Inertia weight can balance the local and global distribution of particle swarm optimization search ability [11]. In order to ensure the global search ability at the beginning of the iteration and the local search ability at the later stage of the iteration, the inertia weight should be gradually reduced with the increase of iteration times.

The two learning factors affect the degree of historical optimization and global optimization of particles, respectively, so the local and global search can be adjusted to balance their capabilities [12]. Small learning factors tend to fall into local optimality, while large learning factors tend to ignore the optimal solution even though they accelerate the convergence speed.

The number of particles affects particle swarm search. Too many particles will improve the information sharing ability between particles, but it will also increase the search time. Too few particles will reduce the communication, leading to the algorithm falling into local optimization. The maximum flight speed of the particle determines the moving distance of the particle and the search ability of the algorithm [13]. The faster the speed, the stronger the search ability, but it is easy to miss the optimal solution. The slower the reading, the stronger the development ability, but it is easy to fall into local optimum. In addition, the range of particles, the termination condition, and fitness function of the algorithm will also affect the optimization results, which need to be determined according to the specific situation of the problem.

2.1.3. Convergence Analysis and Deficiency. If the current position, historical optimal position, and global optimal position of a particle are the same, then the particle cannot approach the optimal position because its inertia weight and speed are not zero, so the algorithm cannot converge [14]. If the inertia weight and velocity are very close to zero, the particles can approach the optimal position, but the diversity of the population will be affected [15]. Because almost all particles will gather in the same optimal position, the optimization will be stagnant and unable to find the global optimal value. It is not advisable for particles to keep the initialization speed and iterate until the end of the algorithm, because the historical optimal and global optimal of particles cannot work, which will reduce the adaptability of the algorithm. This also shows that if the algorithm does not find the global optimal solution before convergence, premature convergence will occur.

The particle iterative optimization of the PSO algorithm inevitably has the defect of only optimizing a part. The local optimal solution will cause the particle to stop searching and communicating with other particles. This will affect the diversity of the population and the optimization results, resulting in the final optimal solution which is not ideal.

2.2. Improved Method of Particle Swarm Optimization Algorithm

2.2.1. Improvement of Inertia Weight. The traditional PSO algorithm uses the inertia weight decreasing strategy to realize the dynamic change of inertia weight, but this method cannot reflect the dynamic search process of particle swarm optimization, and it is easy to lead to the local optimization of the algorithm. Therefore, a sine adjustment strategy with random disturbance appears. Adding sine adjusted inertia weight before and after the search can accelerate the convergence speed of the algorithm [16]. The inertia weight is adjusted according to the following formula:

$$\varpi = \varpi_1 \times \left[1 - \sin\left(\frac{\pi t}{e_{\max}}\right)\right] + r \times \varpi_2 \times \sin\left(\frac{\pi t}{e_{\max}}\right), \quad (6)$$

where r is a random number, $e_{\max}$ is the maximum number of iterations, and ϖ_1, ϖ_2 are the initial inertia weight and the final inertia weight, respectively. After the inertia weight is adjusted according to formula (6), the inertia weight is close to the initial value in the initial iteration of the algorithm, so the global search ability of the algorithm is strong, but the local search ability is weak. In the later stage of iteration, the inertia weight will be close to the final value, which can improve the local search ability and search accuracy.

PSO algorithms with different inertia weights have different balance points in global and local search capabilities [17]. The improved PSO algorithm process of inertia weight increases the threshold and the maximum number of iterations on the basis of the standard PSO algorithm process. When updating the velocity and position of particles, the inertia weight is determined first. When choosing the value of inertia weight, the decreasing strategy is no longer used, but the sine adjustment strategy of random disturbance is adopted.

2.2.2. Improvement of Learning Factors. In the standard PSO algorithm, the value range of two learning factors s_1, s_2 is generally [0, 2] [18]. When solving complex optimization problems, particles at the beginning of iteration are easy to gather together, resulting in the algorithm falling into local optimal value. The dynamic learning factor can help the algorithm avoid local optimization and avoid premature convergence under the premise of accelerating the convergence speed. At the beginning of iteration, if s_1 is larger and s_2 is smaller, the ability of particles of learning themselves can be strengthened and a large number of particles can be avoided. At the later stage of iteration, if s_1 is smaller and s_2 is larger, it can enhance the ability of particles of learning groups and quickly and accurately finding the global optimal solution [19].

The value of learning factor is determined on the basis of formulae (3) and (4). At that time, the values of the two learning factors were as follows:

$$\begin{aligned} s_1 &= 0.6 \times u^{\left(\begin{matrix} e_{\max} - e \\ e_{\max} \end{matrix}\right)}, \\ s_2 &= 0.4 + 0.1 \times r. \end{aligned} \tag{7}$$

When $e > 0.6 \times e_{\max}$, the values of the two learning factors are as follows:

$$\begin{aligned} s_1 &= 0.4 + 0.1 \times u, \\ s_2 &= 0.6 \times u^{\left(\begin{matrix} e \\ e_{\max} \end{matrix}\right)}, \end{aligned} \tag{8}$$

where u is a random number. This improvement can improve the convergence speed of the algorithm at the beginning of the iteration and the accuracy of the solution in the late iteration. Based on the standard PSO algorithm, the improved PSO algorithm process also increases the threshold and the maximum number of iterations. When updating the velocity and position of particles, the two learning factors are determined first. Instead of fixed values, the dynamic changes of learning factors are realized by adding random numbers according to the maximum iterations of particles.

2.2.3. Improvement of Differential Evolution Algorithm. The differential evolution (DE) algorithm performs random search based on population differences [17]. Firstly, the initial population is generated randomly and evenly, and m individuals are randomly generated in N-dimensional space. Then, three individuals x_{v1}, x_{v2}, x_{v3} are randomly selected from the feasible solutions for mutation operation. The mutation individuals are shown in the following formula:

$$b_{ij}(k) = x_{v1j} + F\left(x_{v2j} - x_{v3j}\right). \tag{9}$$

where F is the scaling factor. In order to increase the diversity of feasible solutions, cross operation is carried out, as shown in the following formula:

$$c_{ij}(k+1) = \begin{cases} b_{ij}(k), & \text{if rand}(0,1) \le p \text{ or } j = \text{rand}(1,n), \\ x_{ij}(k), & \text{if rand}(0,1) > p \text{ or } j \ne \text{rand}(1,n), \end{cases} \tag{10}$$

where p is the crossover probability and the value range is [0, 1]. Then, select and update the target individual, as shown in the following formula:

$$x_i(k+1) = \begin{cases} c_i(k+1), & \text{if } f\left(c_i(k+1)\right) < f\left(c_i(k)\right), \\ x_i(k), & \text{if } f\left(c_i(k+1)\right) \ge f\left(c_i(k)\right). \end{cases} \tag{11}$$

The mutation, crossover, and selection operations are repeated until the convergence accuracy of the algorithm meets the requirements or the iteration times meet the termination conditions. The DE algorithm is used to improve the PSO algorithm. In the specific operation, the mutation, crossover, and selection operations in DE algorithm are used to mutate the historical optimal position of particles, so as to maintain the diversity of particles and avoid the weakening of global search ability in the late iteration stage and the emergence of premature scene. In order to judge the aggregation degree of particles, the particle aggregation factor is introduced into the basic PSO algorithm, as shown in the following formula:

$$d(e) = \frac{\min\left(y\left(p_g(e)\right), \overline{y}\right)}{\max\left(y\left(p_g(e)\right), \overline{y}\right)}, \tag{12}$$

where $y(p_g(e))$ is the fitness value of the historical optimal position, e is the current iteration number, and $\overline{y}$ is the average of the current fitness of the particle. The value range of aggregation factor is (0, 1], and the value is directly proportional to the degree of aggregation. In other words, the smaller the value, the lower the aggregation degree of particles and the greater the diversity of particle swarm [20, 21].

Improved PSO algorithm flow based on DE algorithm on the basis of standard PSO algorithm, after calculating the historical optimal position and fitness value, the calculation of aggregation factor, and mutation operation of historical optimal position are added, and then the position and speed of particles are updated according to aggregation factor and mutation operation. In this way, the diversity of particles can be maintained throughout the iteration process, the global search ability can be improved, and the optimization results can be optimized.

2.3. Sliding of Saturated Rock Slope

2.3.1. Monitoring Technology of Saturated Rock Slope Slip. The geophysical methods for slope monitoring include radioactive measurement method, seismic exploration method, ground penetrating radar, and acoustic emission technology [22]. The radioactive measurement method can determine the geological form of slope slip by monitoring radon and its daughters in rock slope. It has the advantages of simplicity and economy, but the results are easily affected

by many factors and the accuracy is not high. In order to excite seismic wave, seismic exploration company uses reflection and refraction signal of seismic wave to judge the nature and shape of rock. Ground penetrating radar (GPR) is similar to seismic exploration, which uses the reflected signal of electromagnetic wave to find the position of slope slip. Through the monitoring of two closely connected acoustic emission probes, acoustic emission technology can judge the position of slope sliding and the time of slope sliding according to the intensity of acoustic emission.

The surface deformation morphology monitoring methods for slope monitoring include digital close range photogrammetry, global positioning system, geographic information system, and remote sensing and telemetry system [23]. Digital close range photogrammetry compares the pictures of the same position in different time periods and then uses computer processing technology to sort out and analyze the data to determine the relevant value of slip. The global positioning system (GPS) can locate and monitor the rock slope from multiple angles and in all directions and has the advantages of high accuracy and efficiency. The digital map of GIS can explore, analyze, and process huge geographic data. It can not only analyze the stability of rock, but also predict the stability of potential rock slope slip area. Remote sensing system uses remote sensing sensor device to survey and monitor large area of landform and geological disasters.

The deep deformation morphology detection methods for slope monitoring mainly include inclinometer technology, strain tube monitoring technology, and time domain reflection technology [24]. The inclinometer uses the movement law of the pendulum under the action of gravity, measures the relevant angle and horizontal displacement data, calculates the deformation trend and depth, and has high measurement accuracy. The strain tube monitoring technology can judge the deep displacement of the slope by monitoring the resistance change of the resistance strain gauge embedded in the strain tube in the slope body. Time domain reflectometry (TDR) is used to collect and analyze the reflected and projected signals of electromagnetic wave to monitor the stability of slope.

2.3.2. Stability Analysis of Saturated Rock Slope. The Swedish circular arc method considers that the ratio of the shear strength of the whole slip surface to the actual shear stress is the stability safety factor, which has the advantages of easy implementation and practical application [25]. In a homogeneous cohesive rock slope, l is a slip arc, and its center and radius are o, r, respectively. The antisliding moment $c \cdot l \cdot R$ on the slip arc and the reaction force caused by the self-weight of the sliding rock are N_R. When the internal friction angle between reaction force and rock is 0, the stability safety factor is shown in the following formula:

$$F_s = \frac{N_R}{N_s} = \frac{c \cdot l \cdot R}{wk}. \tag{13}$$

Among them, the rotational moment $N_s = wk$, w is the self-weight of the sliding rock, and k is the horizontal distance from the vertical line of the rock center to the center of the circle.

The Bishop method takes into account the effect of interslice forces, assuming that the vertical shear forces on both sides of the soil strip are the same, but the direction is opposite. The total normal force and tangential resistance at the bottom of soil strip are z_i, t_i, respectively. The equilibrium condition of vertical force of each soil strip is shown in the following formula:

$$w_i + q_i - q_{i+1} - z_i \cos\ \alpha_i - t_i \sin\ \alpha_i = 0, \tag{14}$$

where w_i is the self-weight and q_i is the tangential interstrip force. The tangential resistance at the bottom of the soil strip is shown in the following formula:

$$t_i = \frac{c_i' g_i}{F_s} + \frac{N_i - \mu g_i}{F_s} ad\phi'. \tag{15}$$

In limit equilibrium, the overall moment equilibrium condition is shown in the following formula:

$$\sum w_i q_i + \sum v_i e_i - \sum t_i r = 0, \tag{16}$$

where v is the horizontal force. The stability safety factor under Bishop method is shown in the following formula:

$$F_s = \frac{\sum (1/m_{\alpha i}) [c_i' g_i + (w_i - \mu_i g_i) ad\phi']}{\sum w_i \sin\ \alpha_i + \sum v_i (e_i / r)}. \tag{17}$$

2.3.3. Numerical Analysis Method of Saturated Rock Slope. The numerical analysis method mainly depends on the constitutive relation of materials to analyze the slip of rock slope, which can solve the slip field and stress field of the slope and can also simulate the specific process of the slip. The commonly used numerical analysis methods include finite element method, discrete element method, fast Lagrangian method, and boundary element method [26]. In the finite element method, the wireless element problem is discretized into a finite element problem, and then it is solved. The function equation is established and analyzed. The application of finite element method in slope mainly includes finite element arc search method and finite element strength reduction method. This method has the advantages of strong applicability and high authenticity of stress calculation, but the workload of calculation is very large and it is easy to make mistakes.

The discrete element method (DEM) discretizes the research object into rigid units and uses the central difference method to solve the motion equation. The result is the motion state of the research object. This method can solve the problem of large displacement of rock mass and simulate the process of rock sliding. The principle of the fast Lagrangian method is consistent with that of the discrete element method, but, compared with the discrete element method, it can be applied to the nonlinear solution of various boundary conditions and constitutive models. Although the solution speed is fast, the accuracy is not high.

The boundary element method transforms the partial differential equation into the boundary integral equation

and then discretizes it into an algebraic equation with only boundary nodes to solve the unknown variables. The algorithm can reduce the dimension of the problem, so it greatly reduces the calculation workload and improves the efficiency. But, when dealing with nonlinear problems, the performance is poor. Sometimes, the results are complex and not clear enough.

3. Experiments on Numerical Simulation of Rock Slope Sliding Based on PSO Algorithm

3.1. Improvement of Particle Swarm Optimization Algorithm. Although the improved PSO algorithm based on DE algorithm mentioned in Chapter 2 can improve the global search ability, it needs a strong local search ability in the later stage of iteration. Simplex method has a small amount of computation. It has the advantages of strong local search ability and fast convergence speed, but poor convergence characteristics. It is difficult to achieve good optimization results only by using simplex method when solving complex functions with higher dimensions. Therefore, on the basis of optimizing the global search capability based on DE algorithm, this paper also uses the simplex method to optimize the local search capability of PSO algorithm.

The flow of the improved algorithm is as follows: firstly, the parameters of particle swarm are initialized, and then the fitness value of each particle is calculated. The second step is to calculate the historical optimal value and global optimal value of particles and update the position and velocity of particles. The third step is to calculate the aggregation factor of particles. If it is greater than 0.1, the DE algorithm is used for mutation, crossover, and selection to update the historical optimal position of particles. In the fourth step, after the fitness values of particles are arranged in ascending order, the first few particles are selected to form a simplex, and simplex search is carried out to update the historical optimal position of particles. The fifth step is to judge whether the termination condition is satisfied. If it is satisfied, the algorithm will be terminated. If not, it will return to the second step to repeat the search.

3.2. Stage Analysis of Rock Slope Sliding. The first is the elastic deformation stage, the rock slope under the load force of instantaneous deformation. Then, in the initial deformation stage, the structural planes and pores in the rock body are gradually closed under the action of sliding force, resulting in elastic aftereffect deformation. The third stage is isokinetic deformation stage, in which the material of rock slope shows viscous damage or creep damage, and the deformation develops at constant speed. The fourth stage is the accelerated deformation stage. Plastic damage and viscous damage appear simultaneously in the rock slope, and the deformation speed will accelerate with time. The last stage is the instability stage, the deformation of the slope presents a steep increase and failure situation, the cracks in the slope spread to the maximum, and the duration of the instability stage is relatively short.

3.3. Numerical Simulation of Rock Slope Slip. The slip of rock slope was simulated numerically by ABAQUS software, the stability of rock slope was analyzed by finite element method, and all data were analyzed by the improved PSO algorithm in this paper. The Mohr-Coulomb model of ABAQUS software can simulate the main characteristics of rock and can be used to analyze transversely isotropic rock slope. The finite element analysis model of rock slope has a slope height of 45 m and a slope angle of 40°. The physical property parameters of the material are the common sandy mudstone with density of 2.44 g/cm^3, elastic modulus of 1.21×10^4 mpa, and porosity of 5.42%. After confirming the model data and material parameters, the model was established by ABAQUS software. The top, middle, and foot of the slope are selected as feature points to judge whether the slope is sliding.

In order to analyze the effect of rockfall impact on rock slope slip, lS-DYNA program is used to simulate rock slope with rockfall impact. Assuming that the rock slope under impact has uniform texture and fixed boundary, the rockfall in the simulated value is a rigid cube, and then the rockfall drop model is established.

4. Discussion on Results of Numerical Simulation Analysis

4.1. Performance of the Improved Algorithm in This Paper. The convergence performance of improved algorithm (TP-PSO), standard PSO algorithm, and improved PSO algorithm based on DE algorithm (DE-PSO) is compared and analyzed.

As shown in Figure 2, the improved PSO algorithm converges after nearly 100 iterations, and the improved PSO algorithm based on DE algorithm converges after 150 iterations, while the standard PSO algorithm shows a slow convergence trend. Therefore, in terms of convergence speed, the improved PSO algorithm is better than the improved PSO algorithm based on DE and the standard PSO algorithm.

The performance of the algorithm is also reflected in the optimization effect. Therefore, the optimization results of the test function under different algorithms are compared. The optimal value results obtained by the three algorithms are as follows:

As shown in Table 1, the optimization results of TP-PSO algorithm in four functions are 3.5712, 0.0572, 5.0417, and 2.2401. In different test functions, the optimal values obtained by different algorithms are not consistent, and they are greatly different due to the characteristics of the function itself.

As shown in Figure 3, the minimum optimization result of TP-PSO algorithm is 0.0572 and the maximum is 5.0417. The minimum optimization result of DE-PSO algorithm is 0.0275 and the maximum is 15.3622. The minimum and maximum results of PSO algorithm are 2.8083 and 19.7796, respectively. This shows that the accuracy of TP-PSO algorithm is higher than that of DE-PSO algorithm and PSO algorithm.

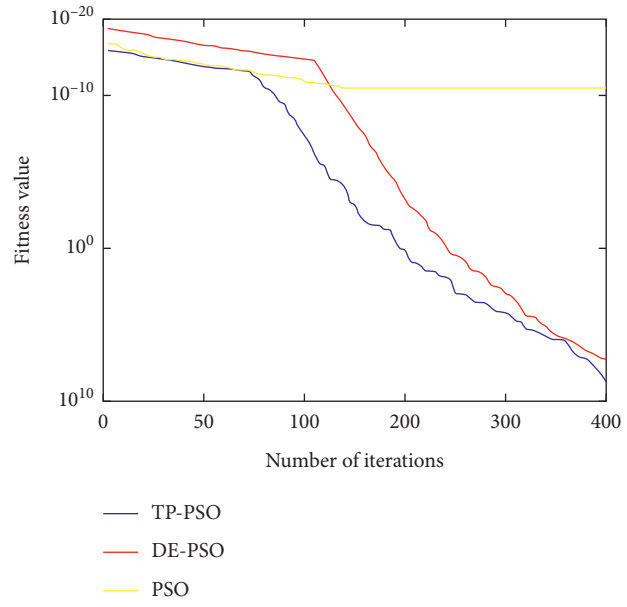

Figure 2: Convergence curve of the algorithm.

Table 1: Optimal values of different algorithms.

Algorithm	Function 1	Function 2	Function 3	Function 4
TP-PSO	3.7512	0.0572	5.0417	2.2401
DE-PSO	2.0458	15.3622	9.1219	0.0275
PSO	2.8083	3.6157	19.7796	19.4803

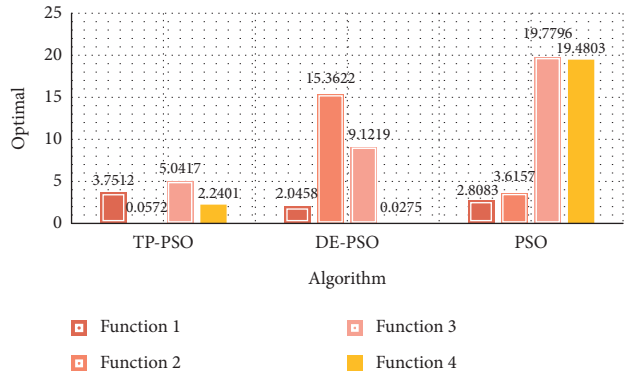

Figure 3: Comparison of optimal values of different algorithms.

4.2. Numerical Simulation Results of Rock Slope Slip. In this paper, the stability of rock slope is analyzed by numerical simulation of finite element method. Three main sections of the top, middle, and foot of the slope are selected to calculate the instability probability of the left and right sides of each main section. The results are as follows:

As shown in Table 2, the maximum failure probability of the left and right sides of the main section at the top of the slope is 0.1789 and 0.1816, and the minimum probability of instability is 0.0021 and 0.0059. However, in most cases, the instability probability of the left side is slightly higher than that of the right side, and it is impossible to judge which side has the higher instability probability only by the maximum and minimum value.

Table 2: Instability probability of main section at the top of slope.

X_i (m)	$\mu_A(x)$ left	P left	$\mu_A(x)$ right	P right
0	1	0.1789	1	0.1816
1	0.9272	0.1473	0.8924	0.1489
2	0.8815	0.1279	0.7718	0.1147
3	0.8251	0.1056	0.6675	0.0873
4	0.7762	0.0857	0.5781	0.0671
5	0.7264	0.0653	0.5004	0.0481
6	0.6835	0.0510	0.4332	0.0328
7	0.6399	0.0347	0.3753	0.0226
8	0.5907	0.0213	0.3267	0.0142
9	0.5346	0.0021	0.2750	0.0059

As shown in Figure 4, in the main section at the top of the slope, the average instability probability on the left is 0.0820, and the average instability probability on the right is 0.0723. This shows that, in general, the instability probability of the left side is slightly higher than that of the right side. Therefore, for the top of slope, more attention should be paid to the generation of left side slope slip.

Then, the stability of the main section in the middle of the slope is analyzed, and the instability probability of the left and right sides of the main section is calculated.

As shown in Table 3, the maximum instability probability of the left and right sides of the main section in the slope is 0.1557 and 0.1353, and the minimum instability probability is 0.0111 and 0.0029. The variation trend of instability probability of the left and right sides of the main section in the slope is as follows:

As shown in Figure 5, in the main section of the middle slope, the average instability probability on the left side is 0.0772, and that on the right side is 0.0492. This shows that, in general, the instability probability of the left side is higher than that of the right side. Therefore, it is necessary to pay more attention to the left side slope slip for the middle slope.

Then, the stability of the main section at the toe of the slope is analyzed, and the instability probability of the left and right sides of the main section of the toe is calculated.

As shown in Table 4, the maximum failure probability of the left and right sides of the main section at the toe of the slope is 0.1755 and 0.1784, and the minimum probability of instability is 0.0115 and 0.0063. The variation trend of the instability probability of the left and right sides of the main section of the slope toe is as follows:

As shown in Figure 6, in the main section of slope toe, the average instability probability on the left side is 0.0837, and that on the right side is 0.0677. This shows that, in general, the instability probability of the left side is higher than that of the right side. Therefore, for the toe of slope, it is necessary to pay more attention to the left side slope slip.

To sum up, in the three main sections of the top, middle, and toe of the slope, the trend of the instability probability of the top and foot of the slope is similar, and the instability probability of the left side is higher than that of the right side. Although the left side of the slope is higher than the right side, it is relatively stable.

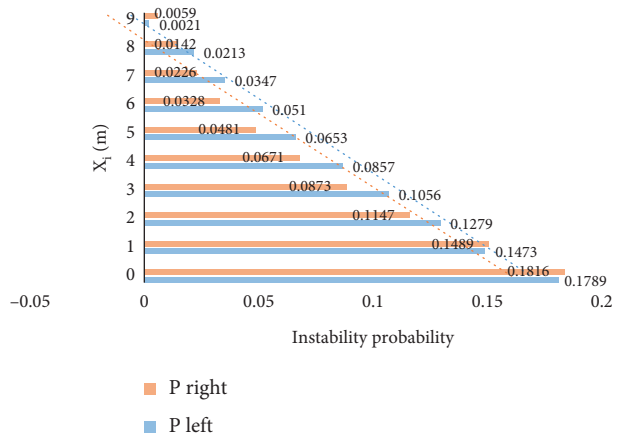

Figure 4: Variation trend of instability probability of main section at the top of slope.

Table 3: Instability probability of main section in middle slope.

X_i (m)	μ_A (x) left	P left	μ_A (x) right	P right
0	1	0.1557	1	0.1353
1	0.9538	0.1489	0.8516	0.1082
2	0.8979	0.1158	0.6963	0.0793
3	0.8452	0.0963	0.5692	0.0574
4	0.7956	0.0785	0.4653	0.0408
5	0.7484	0.0621	0.3804	0.0284
6	0.7051	0.0478	0.3112	0.0191
7	0.6637	0.0347	0.2549	0.0127
8	0.6226	0.0215	0.2081	0.0074
9	0.5860	0.0111	0.1688	0.0029

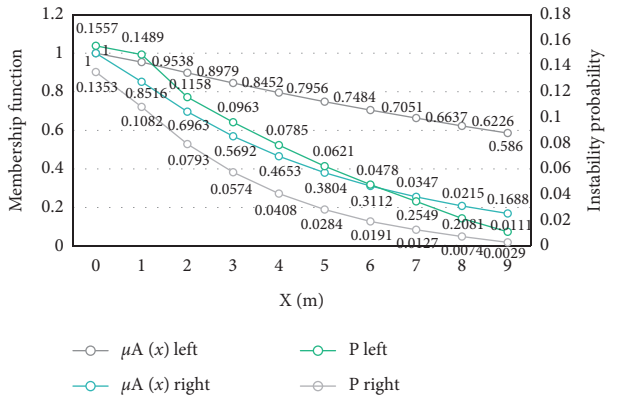

Figure 5: Variation trend of instability probability of main section in middle slope.

4.3. Influencing Factors of Rock Slope Slip

4.3.1. Influence of Rock through Joint. The influence of joint on rock slope slip is analyzed from the same direction through joint and reverse through joint. The same joint parameters are used in the experiment, 5 joints are set in the same direction and 5 joints in the reverse direction, respectively. Starting from the foot of the rock, 5 reference points were selected on average to observe and calculate the

Table 4: Instability probability of main section of slope toe.

X_i (m)	μ_A (x) left	P left	μ_A (x) right	P right
0	1	0.1755	1	0.1784
1	0.9391	0.1519	0.8672	0.1427
2	0.8815	0.1279	0.7512	0.1108
3	0.8272	0.1058	0.6507	0.0847
4	0.7762	0.0857	0.5626	0.0408
5	0.7284	0.0675	0.4884	0.0463
6	0.6835	0.0511	0.4231	0.0325
7	0.6414	0.0364	0.3666	0.0215
8	0.6019	0.0232	0.3176	0.0129
9	0.5648	0.0115	0.2752	0.0063

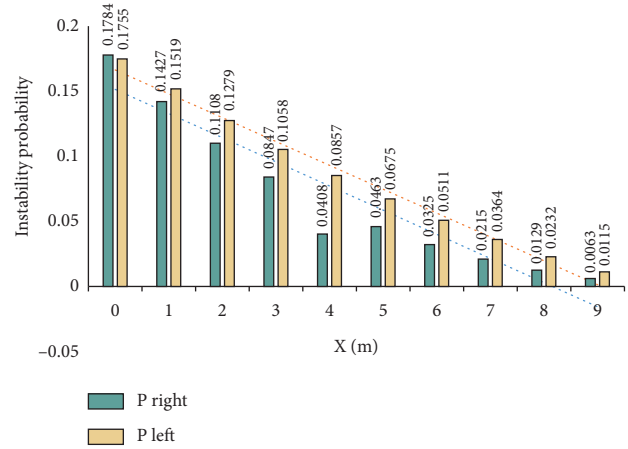

Figure 6: Variation trend of instability probability of main section at slope toe.

displacement of the upper and lower sides and the left and right sides of the reference points.

As shown in Table 5, in the same direction through joint, reference point no. 1 has the largest displacement at the upper and lower sides, which are −5.992 cm and −4.481 cm, respectively; in the reverse through joint, the largest displacement at the upper and lower sides is reference point 3, which is −5.782 cm and −7.626 cm, respectively.

As shown in Figure 7, the relative displacement of no. 1 reference point is the largest, which is 1.511 cm, and the relative displacement of no. 5 reference point is the smallest, which is 0.122 cm. This shows that the rock slope with the same direction through joint is mainly affected by the joint at the toe of the slope and the sliding occurs from bottom to top.

As shown in Figure 8, the relative displacement of no. 3 reference point is the largest, which is 1.656 cm, while the relative displacement of no. 1 reference point is the smallest, which is 0.401 cm. This shows that the rock slope with reverse through joints is mainly affected by the joints in the slope and the sliding occurs from the middle to both ends.

4.3.2. Impact of Rockfall. The influence of rockfall on rock sliding can be analyzed from the impact position, height, and size of rockfall. This study analyzes the height and size of

Table 5: Displacement of reference point.

Reference point	Displacement in the same direction			Reverse displacement		
	Upside	Downside	Relative	Left side	Right side	Relative
1	−5.992	−4.481	1.511	−4.523	−4.122	0.401
2	−5.331	−4.476	0.855	−5.210	−4.258	0.952
3	−4.235	−3.993	0.242	−6.982	−5.326	1.656
4	−3.426	−3.019	0.407	−4.731	−3.877	0.854
5	−2.223	−2.101	0.122	−3.906	−3.019	0.887

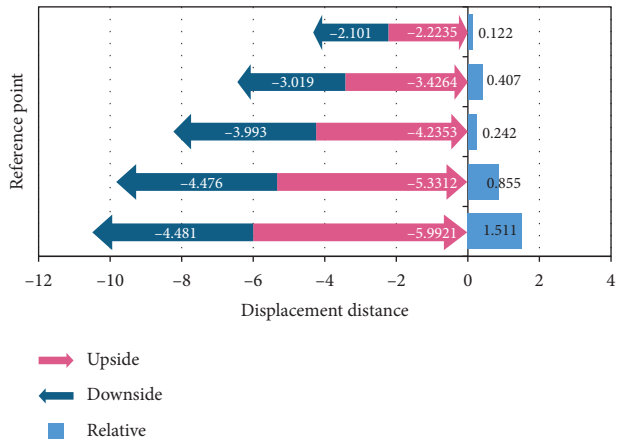

Figure 7: Displacement of reference point through joint in the same direction.

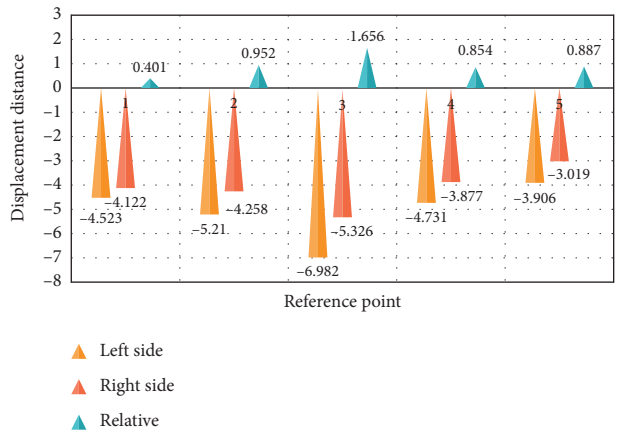

Figure 8: Displacement of reference point of reverse through joint.

rockfall and unifies the material and impact position of rockfall. The total energy of rock slope is analyzed by selecting cubic rockfall with side length of 0.25 m, 0.5 m, 0.75 m, and 1 m, respectively, from the height of 3 m, 6 m, 9 m, 12 m, and 15 m.

As shown in Figure 9, the total energy of a rockfall with a side length of 0.25 m impacting the rock slope at 3 m is the minimum, which is 30019 J. When the rockfall with a side length of 1 m impacts the rock slope at 15 m, the maximum energy is 310252J. The difference between the minimum and the maximum is about 10 times. With the increase of the size and height of rockfall, the total energy of rock slope is also increasing, and the possibility and degree of rock slope sliding are higher.

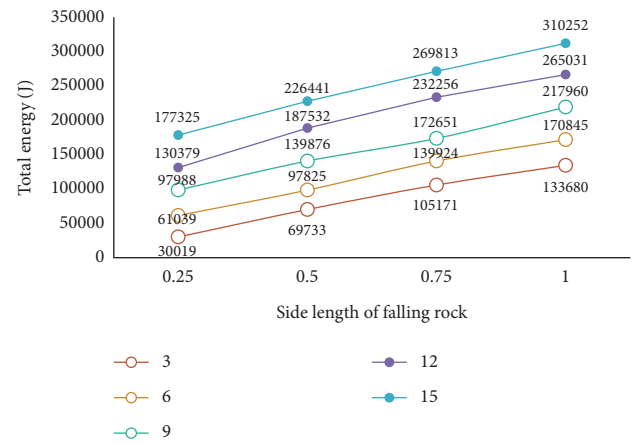

Figure 9: Total energy of rock slope.

5. Conclusions

Particle swarm optimization (PSO) algorithm is bound to fall into local optimization due to its continuous iterative optimization. In this paper, based on DE algorithm and simplex method, the particle swarm optimization algorithm is improved, which improves the global search ability in the initial iteration stage and the local search ability in the late iteration stage. Through comparative analysis, it is found that the algorithm in this paper has faster convergence speed and higher optimization accuracy.

The traditional algorithm is always difficult to improve the analysis efficiency because of the large amount of calculation in the analysis of data of rock slope. The improved algorithm can effectively solve this problem. The stability of rock slope is analyzed by finite element method, and all simulation data are analyzed by improved PSO algorithm. In the sliding model of rock slope constructed in this paper, the instability probability of the left side is higher than that of the right side, and the sliding is more likely to occur. The rock slope with the same direction through joint is mainly affected by the joint at the toe of the slope, and the rock slope with reverse through joint is mainly affected by the joint in the slope, and the sliding occurs from the middle to both ends. In addition, the size and height of rockfall will directly affect the possibility of rock slope sliding.

Due to the limited time and knowledge, there are some deficiencies in this study. The first is the defect of the numerical simulation method itself. There is a big difference between the numerical simulation in the laboratory and the actual situation, so it is difficult to achieve complete

reduction. Secondly, when analyzing the factors affecting slope slip, the condition of unbroken joints and irregular rockfall is not taken into account. These shortcomings in the future research work need to be improved as far as possible, in order to improve the reliability of the data.

Data Availability

No data were used to support this study.

Conflicts of Interest

The authors declare that they have no conflicts of interest.

Acknowledgments

This work was supported by the General Programs of the National Natural Science Foundation of China (Grant no. 51774184).

References

[1] D. P. Deng, L. H. Zhao, and L. Li, "Limit equilibrium analysis for rock slope stability using basic Hoek–Brown strength criterion," *Journal of Central South University*, vol. 1, no. 09, pp. 230–239, 2017.

[2] Y. Deng, "A threat assessment model under uncertain environment," *Mathematical Problems in Engineering*, vol. 2015, Article ID 878024, 12 pages, 2015.

[3] A. Ketabi and M. H. Fini, "Adaptive underfrequency load shedding using particle swarm optimization algorithm," *Journal of Applied Research & Technology*, vol. 15, no. 1, pp. 54–60, 2018.

[4] R. Mohammadi, S. M. T. F. Ghomi, and F. Jolai, "Pre-positioning emergency supplies for earthquake response: a new multi-objective particle swarm optimization algorithm," *Applied Mathematical Modelling*, vol. 40, no. 9-10, pp. 5183–5199, 2016.

[5] X. Zhang, X. Wang, Y. Niu, and G. Cui, "A novel multi-objective particle swarm optimization algorithm based on invasive weed optimization," *Journal of Computational and Theoretical Nanoscience*, vol. 13, no. 6, pp. 3902–3908, 2016.

[6] L. Wang, B. Huang, Z. Zhang, Z. Dai, P. Zhao, and M. Hu, "The analysis of slippage failure of the HuangNanBei slope under dry-wet cycles in the three gorges reservoir region, China," *Geomatics, Natural Hazards and Risk*, vol. 11, no. 1, pp. 1233–1249, 2020.

[7] W. Zhuang, L. I. Chi, and D. Xuan-Ming, "Application of transparent soil model tests to study the soil-rock interfacial sliding mechanism," *Journal of Mountain ence,Journal of Mountain Science*, vol. 16, no. 04, pp. 214–222, 2019.

[8] M. Wang and Q. Tian, "Dynamic heat supply prediction using support vector regression optimized by particle swarm optimization algorithm," *Mathematical Problems In Engineering*, vol. 2016, Article ID 3968324, 10 pages, 2016.

[9] A. Rana and D. Sharma, "Mobile ad-hoc clustering using inclusive particle swarm optimization algorithm," *International Journal of Electronics and Information Engineering*, vol. 8, no. 1, pp. 1–8, 2018.

[10] M. A. Tawhid and K. B. Dsouza, "Hybrid binary dragonfly enhanced particle swarm optimization algorithm for solving feature selection problems," *Mathematical Foundations of Computing*, vol. 1, no. 2, pp. 181–200, 2018.

[11] G. Guan, Q. Yang, W. Gu, W. Jiang, and Y. Lin, "Ship inner shell optimization based on the improved particle swarm optimization algorithm," *Advances in Engineering Software*, vol. 123, pp. 104–116, 2018.

[12] H. Ouyang, Y. Quan, L. Gao et al., "Global hierarchical path planning of mobile robot based on hybrid genetic particle swarm optimization algorithm," *Zhengzhou Daxue Xuebao/ Journal of Zhengzhou University*, vol. 41, no. 4, pp. 34–40, 2020.

[13] M. Alimardani and M. Almasi, "Investigating the application of particle swarm optimization algorithm in the neural network to increase the accuracy of breast cancer prediction," *International Journal of Computer Trends and Technology*, vol. 68, no. 4, pp. 65–72, 2020.

[14] Y. Sun and Y. Gao, "An efficient modified particle swarm optimization algorithm for solving mixed-integer nonlinear programming problems," *International Journal of Computational Intelligence Systems*, vol. 12, no. 2, p. 530, 2019.

[15] J. K. Arthur, E. K. Boahen, F. Doh et al., "Firewall rule anomaly detection and resolution using particle swarm optimization algorithm," *International Journal of Computer Applications*, vol. 178, no. 33, pp. 975–8887, 2019.

[16] D. Wu, Y. Liu, K. Zhou, K. Li, and J. Li, "A multi-objective particle swarm optimization algorithm based ON human social behavior for environmental economics dispatch problems," *Environmental Engineering and Management Journal*, vol. 18, no. 7, pp. 1599–1607, 2019.

[17] G. Chinnadurai and H. Ranganathan, "Curvature based 2 wheels self supporting robot based on the particle swarm optimization algorithm," *International Journal of Computing & Information Technology*, vol. 11, no. 1, pp. 37–43, 2019.

[18] N. R. Zhou, A. W. Luo, and W. P. Zou, "Secure and robust watermark scheme based on multiple transforms and particle swarm optimization algorithm," *Multimedia Tools and Applications*, vol. 78, no. 2, pp. 2507–2523, 2019.

[19] D. Li, K. Li, J. Liang, and A. Ouyang, "A hybrid particle swarm optimization algorithm for load balancing of MDS on heterogeneous computing systems," *Neurocomputing*, vol. 330, pp. 380–393, 2019.

[20] J. Liu, Y. Guo, S. Zha et al., "Multi station assembly sequence planning based on improved particle swarm optimization algorithm," *Jisuanji Jicheng Zhizao Xitong/Computer Integrated Manufacturing Systems, CIMS*, vol. 24, no. 11, pp. 2701–2711, 2018.

[21] J. Guan and L. Jia, "A multi-objective particle swarm optimization algorithm for solving human resource allocation problem," *IPPTA: Quarterly Journal of Indian Pulp and Paper Technical Association*, vol. 30, no. 8, pp. 144–149, 2018.

[22] K. Y. Yang, C. X. Chen, K. Z. Xia et al., "Research on sliding failure mechanism of gently inclined bedding compound rock mass slope under hydraulic drive," *Zhongguo Gonglu Xuebao/ China Journal of Highway and Transport*, vol. 31, no. 2, pp. 144–153, 2018.

[23] L. Xinrong, H. Chunmei, H. Chunmei, L. Xingwang, L. Gang, and Z. Bin, "Study on the safety factors of the bedding rock slope under dynamic loading," *Journal of Engineering Science and Technology Review*, vol. 2016, no. 3, pp. 161–175, 2016.

[24] Z. Li, H. U. Zheng, L. Wenlian et al., "Plastic limit analysis of open-pit mine jointed rock slope considering translation-rotation mechanisms," *Yanshilixue Yu Gongcheng Xuebao/ Chinese Journal of Rock Mechanics and Engineering*, vol. 37, no. s2, pp. 4056–4068, 2018.

[25] C. Wen, X. Jiang, H. Yang et al., "Influence of slope conditions on seismic displacement modes of gravity retaining wall,"

Journal of Vibration,Measurement & Diagnosis, vol. 37, no. 4, pp. 763–768, 2017.

[26] D. Mercier, J. Coquin, T. Feuillet et al., "Are Icelandic rock-slope failures paraglacial? Age evaluation of seventeen rock-slope failures in the Skagafjörður area, based on geomorphological stacking, radiocarbon dating and tephrochronology," *Geomorphology*, vol. 296, pp. 45–58, 2017.